JTTEE5 19:816–823
DOI: 10.1007/s11666-010-9479-y
1059-9630/$19.00 © ASM International

Microstructure and Phase Composition of Composite Coatings Formed by Plasma Spraying of ZrO_2 and B_4C Powders

P. Karuna Purnapu Rupa, Prashant Sharma, R.M. Mohanty, and K. Balasubramanian

(Submitted April 22, 2009; in revised form January 18, 2010)

The effect of addition of 5 to 30 wt.% boron carbide (B_4C) on structure and hardness of plasma sprayed zirconia (ZrO_2) coating has been studied in this paper. The coatings have exhibited a uniform porous microstructure. A reaction between B_4C and ZrO_2 resulted in the formation of a diboride (ZrB_2) phase. The presence of ZrB_2 in the coatings has been confirmed through x-ray diffraction studies. In order to study the effect of critical processing parameters, the coatings have also been deposited under increased hydrogen flow rate (11.8 SLM). This increased the abrasion integrity of the coatings. A high yield of ZrB_2 was observed in the case of 15 wt.% B_4C addition. Hardness of the coatings have been influenced by the porosities, additionally generated by the formation of ZrB_2. Under increased hydrogen flow rate, a composite coating of ZrO_2-ZrB_2 was obtained from the ZrO_2-B_4C powder mixture.

Keywords boron carbide, composite coatings, plasma spray, zirconia, zirconium boride

1. Introduction

Controlled atmospheric plasma spraying (APS) is being used as a coating process to enhance the performance of substrate materials at extreme environments by the surface modification. In this process, powder particles are melted, accelerated in the plasma and are deposited on the substrates as thin lenticular features known as splats. With time the continuous deposition of splats results in the formation of a coating with a distinct microstructure and properties. The materials for plasma spray include oxides ceramics such as Al_2O_3 and ZrO_2, metals and alloys such as nickel-chromium and intermetallics such as NiAl, AlN, etc. In APS parameters, such as particle size, particle size distribution, particle density, electric power, primary and secondary gas flow rates, particle in-flight time and stand-off distance all play an important role in obtaining a coating with desired set of properties. For this, process maps have been developed as a guide to obtaining the desired coating properties and also to improve the reproducibility and reliability (Ref 1, 2). These have been extensively studied for single phase metals/alloys and ceramics. Selected composites, such as WC-Co (Ref 3) and Al_2O_3-TiO_2 (Ref 4) coatings, also have been obtained using APS. The number of process variables increases as two or more powders with different thermo-physical properties interact with the plasma. A variant of composite coatings is reactive plasma spray (RPS) coatings where a reaction takes place between the precursor particles and the plasma or between powder particles in the plasma. Examples of the RPS where a reaction takes place between precursor particles and the plasma include the formation of TiN (Ref 5, 6), AlN (Ref 7), Si_3N_4 (Ref 8), Fe_4N (Ref 9) and CrN (Ref 10) in N_2/Ar plasmas, the reaction of aluminum metal powder in $TiCl_4$ plasma to produce TiAl and Ti_3Al (Ref 11) and the reaction of molybdenum particles with disilane plasma to form $MoSi_2$ (Ref 11). The examples of RPS as a result of reaction between powder particles in inert plasma include that of TiC (Ref 12), TiAl (Ref 13), NiAl (Ref 14), etc. In addition to the above, the RPS has also been used to obtain metal matrix composites with hard phases formed in situ such as TiC-Fe (Ref 15, 16), Fe_2O_3-Al (Ref 17) and TiN-Ti (Ref 18). Ceramic matrix composite coatings of Al_2O_3-TiB_2 have been obtained by RPS with Al-Si, TiO_2 and B_2O_3 precursor particles (Ref 19). The majority of the RPS coatings involve combustion synthesis wherein the heat of the plasma is utilized to initiate the reaction. The advantage is that once ignited the exothermic reactions are self-propagating, converting the reactant particles into useful products. The nature of these reactions is exothermic and under steady state mode the combustion wave front moves with a uniform velocity which varies from 0.001 to 0.15 m s^{-1} (Ref 20). In contrast to this, the available literature on the in situ synthesis of ceramic matrix composites which occur by conventional reduction type reactions is scarce. The reaction between ZrO_2 and B_2O_3 in the presence of carbon or between ZrO_2 and B_4C to produce ZrB_2 is an example of a reduction reaction which is highly endothermic and requires high

P. Karuna Purnapu Rupa, Prashant Sharma, R.M. Mohanty, and **K. Balasubramanian**, Non Ferrous Materials Technology Development Centre, Kanchanbagh, Hyderabad 500058, India. Contact e-mails: rmmohanty@nftdc.res.in and mohantyrm@yahoo.com

temperatures (~2000 °C) for prolonged time periods (2-5 h) (Ref 21). RPS could be of great advantage for obtaining coatings of such systems as the temperatures involved in plasma spray are very high (~6000-15000 °C). These high temperatures may significantly reduce the time required for reaction. The Zr-O-B system has been studied by Mizusako et al. by using electro thermal explosion spraying where the authors have used Zr and B_2O_3 powders as precursors (Ref 22). However, the reaction between Zr and B_2O_3 is exothermic. This exothermicity assists in sustaining the reaction initiated by the resistive heating of Zr and B_2O_3 and leads to the formation of the product phases. In the present investigation, the authors focused on RPS of ZrO_2 and B_4C powders to produce composite coatings under two process conditions. ZrO_2 is a very stable oxide, good thermal insulator with high-fracture toughness. It is extensively used as a thermal barrier coating. B_4C is extremely hard and gives reliable wear and abrasion resistance. The reaction product, ZrB_2, is a transition metal boride with very high melting point and high hardness. Due to its excellent mechanical and thermal properties, ZrB_2 is being considered for use as a high-temperature structural material. ZrB_2 has high thermal shock and thermal fatigue resistance which makes it a candidate material for aerospace applications (Ref 23). In this paper, the effect of the relative amounts of B_4C and ZrO_2 powders and the process conditions on the microstructure of the composite coatings as well as the formation of ZrB_2 is discussed.

2. Experimental Details

2.1 Deposition Parameters

AISI 304, a versatile austenitic steel, was used in this study as a substrate for the composite coatings. Prior to plasma spraying of the composite powders, the AISI 304 substrates of dimensions 20 × 20 × 5 mm were blasted with 100 μm Al_2O_3 grits and the surfaces were cleaned through ultrasonication process. The average roughness of the substrates after the grit-blasting process was 3.2 μm. A mixture of ZrO_2 (8 mole% yttria stabilized, Metco 204 NS, Westbury, NY) and B_4C (Vajrabor®, Mumbai, India) powders was prepared by adding 5, 10, 15, 20 and 30 wt.% of B_4C to ZrO_2. To ensure the uniform distribution of the particles, these powders were mixed with 10% polyvinyl alcohol in planetary ball mill (Fritsch, Germany) for 1 h and then oven dried for 2-3 h. The agglomerated powders were then sieved through −230 mesh. The powder mixtures obtained as above were sprayed on the AISI 304 substrate through Metco 3M (Metco, Westbury, NY) plasma spray equipment. The argon and hydrogen flow rate were 35.4 and 7.08 SLM, respectively. The plasma current and voltage were 500 A and 50 V, respectively. A spray distance of 100 mm was fixed. To study the effect of plasma conditions, the agglomerated powder mixture was sprayed at an argon flow rate of 35.4 SLM and increased hydrogen flow rate of 11.8 SLM retaining all other parameters constant. A ZrO_2 coating was also sprayed under these conditions for comparison with the composite coatings. Direct spraying of the composite powders on the substrates resulted in the delamination of the coatings. Thus, nickel-chromium (Ni20Cr, Metco 43F-NS, Westbury, NY) was sprayed as bond coat on the AISI 304 substrate. The thickness of the bond coat was 80 μm. Nickel-chromium bond coat prevented the delamination of the coatings. The thickness of the plasma sprayed composite coatings on the bond coat was ranging from 200 to 300 μm. The thicknesses of the coatings were measured using a Psoitest® DFT (DeFelsko, Ogdensberg, NY) coating thickness gauge. The phase analysis of the coatings was carried out by an x-ray diffraction (XRD) system (X'Pert, Panalytical, Almelo, The Netherlands). The microstructures of the deposited coatings were studied using a scanning electron microscope (SEM) (TESCAN VEGA LSII, Brno, Czech) having an energy-dispersive x-ray microanalysis detector (EDAX) (INCA X-sight, Oxford Instruments, UK). Vickers hardness measurement was done using a microhardness tester (HSV-20, Shimadzu, Kyoto, Japan). Five indentations were performed on each coating. Details on the various samples and the designations used to identify them throughout this text are given in Table 1 and 2.

Table 1 Sample designation and spray parameters for series 1

Sample designation	Powder composition		
S5	ZrO_2 + 5 wt.% B_4C	Argon	35.4 SLM
S10	ZrO_2 + 10 wt.% B_4C	Hydrogen	7.08 SLM
S15	ZrO_2 + 15 wt.% B_4C	Current	500 A
S20	ZrO_2 + 20 wt.% B_4C	Voltage	50 V
S30	ZrO_2 + 30 wt.% B_4C	Spray distance	100 mm

Table 2 Sample designation and spray parameters for series 2

Sample designation	Powder composition		
SH5	ZrO_2 + 5 wt.% B_4C	Argon	35.4 SLM
		Hydrogen	11.8 SLM
SH15	ZrO_2 + 15 wt.% B_4C	Current	500 A
		Voltage	50 V
SH30	ZrO_2 + 30 wt.% B_4C	Spray distance	100 mm

2.2 Powder Morphology

The particle size analysis was carried out by a particle size analyzer (CILAS 1064, Marcoussis, France) with an analysis range of 0.04-500 μm. The SEM micrographs and size distribution of the particles used for spraying of ZrO_2 and B_4C composite coatings are shown in Fig. 1. The ZrO_2 particles were spherical in appearance whereas that of the B_4C particles were lathe or platelet shaped. The mean particle size (d_{50}) of ZrO_2 and B_4C were 55 and 7.5 μm, respectively. The agglomerated powder mixtures for 5, 15 and 30 wt.% B_4C addition are shown in Fig. 2(inset). The powder mixture was collected from the external powder port, mounted near the anode nozzle exit, for particle size

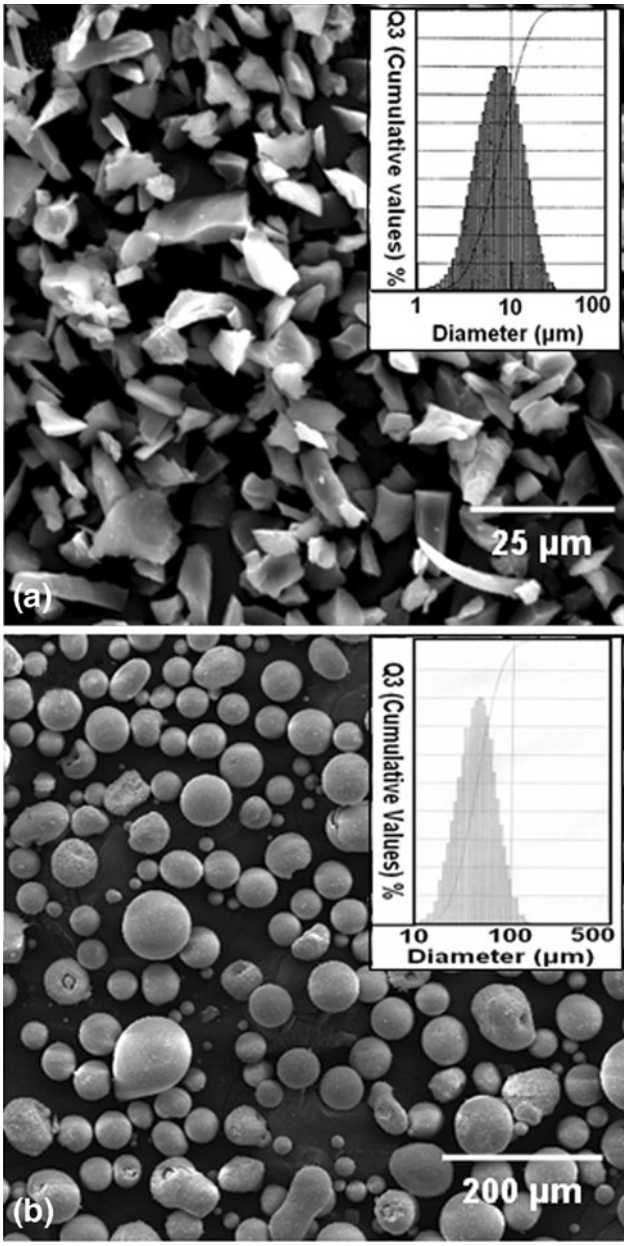

Fig. 1 Particle morphologies and size distribution and size of (a) B_4C and (b) ZrO_2 powders. The insets show the corresponding histogram for particle size distribution

analysis. The size analysis, using water as the dispersing medium, of the powder mixture before it interacts with plasma is shown in Fig. 2. A bimodal distribution was observed with the ratio of finer to larger particles increasing as the B_4C content increased from 5 to 30 wt.% B_4C.

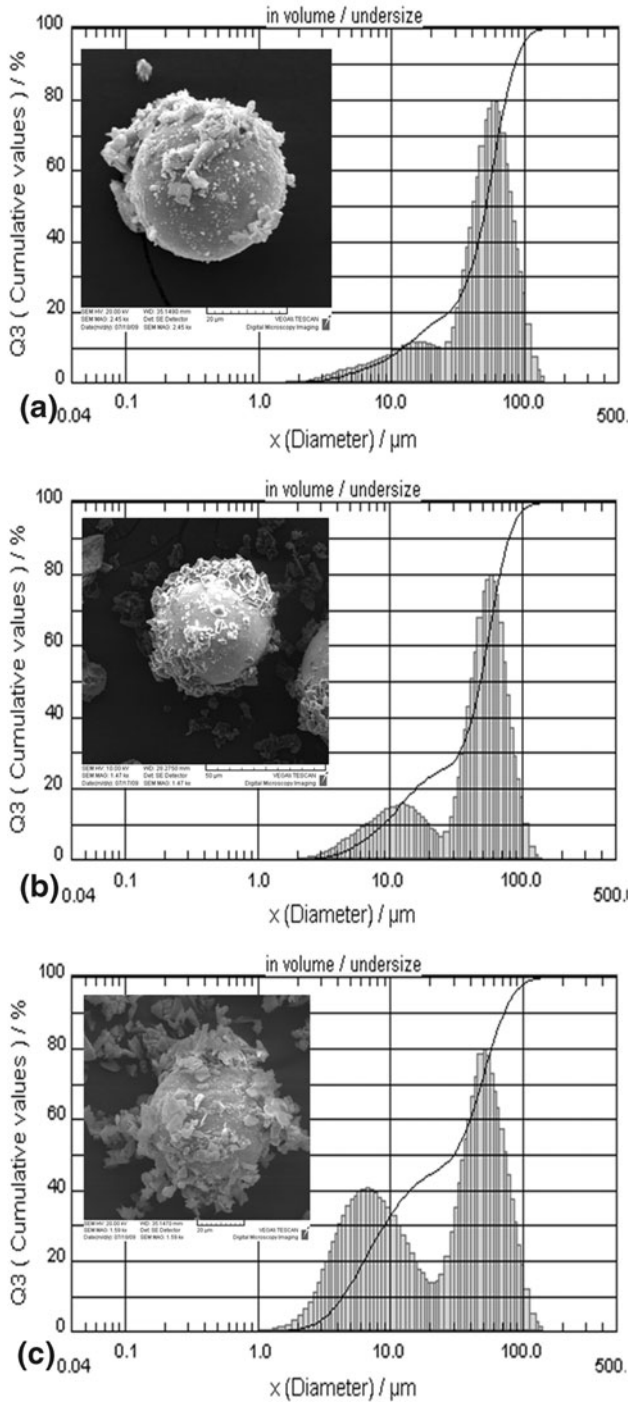

Fig. 2 Agglomerated powder mixture (insets) of (a) 5, (b) 15, and (c) 30 wt.% B_4C addition to ZrO_2. The histograms show the particle size distribution of the powder mixture collected from the powder port of the plasma system

3. Results

3.1 Microstructure and Phase Formation

Figure 3 shows the microstructures of the as-sprayed coatings designated as S5, S15 and S30, deposited at plasma gas flow rates of 35.4 SLM Ar and 7.08 SLM H_2. It is observed from Fig. 3 that all the coatings are characterized by a highly porous microstructure. APS coating microstructures are normally characterized by splats. In the case of S5 coating, the splats are seen, along with the presence of a uniform distribution of fine particles in the

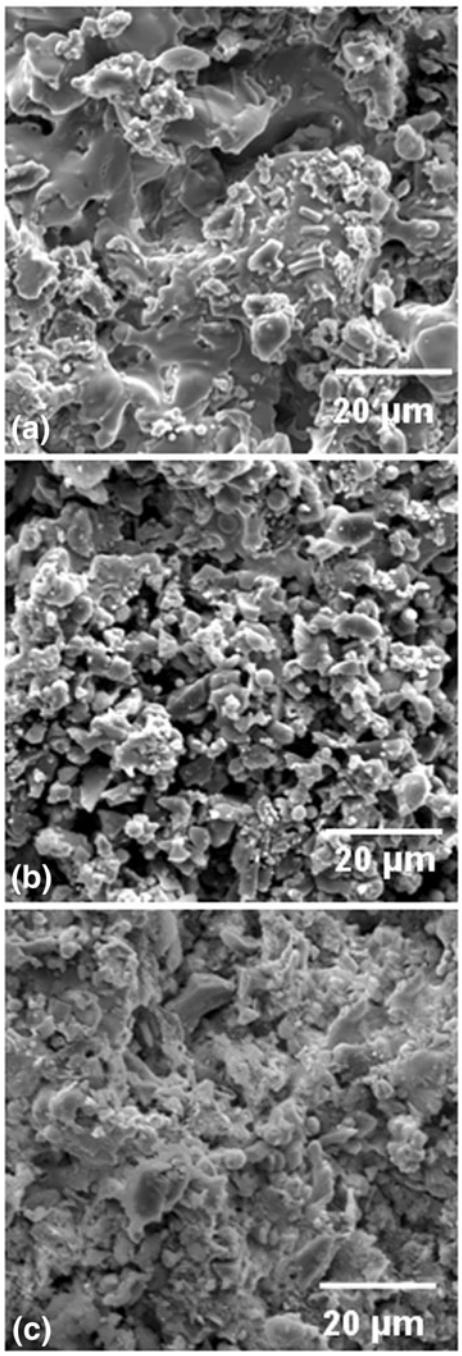

Fig. 3 Surface microstructure of as plasma sprayed coatings with (a) 5, (b) 15, and (c) 30 wt.% B_4C addition to ZrO_2

microstructure (Fig. 3a). Figure 4 shows the x-ray diffraction (XRD) patterns for coatings of S5-S30. For S5, the XRD pattern revealed the presence of tetragonal ZrO_2 (JCPDS: 82-1242), monoclinic ZrO_2 (JCPDS: 74-0815), zirconium diboride (ZrB_2) (JCPDS: 75-0964). No B_4C peaks were detected in this pattern. XRD of the milled and agglomerated powder did not show the presence of ZrB_2. It indicates that a reaction has occurred between B_4C and ZrO_2 to form ZrB_2 during spraying and

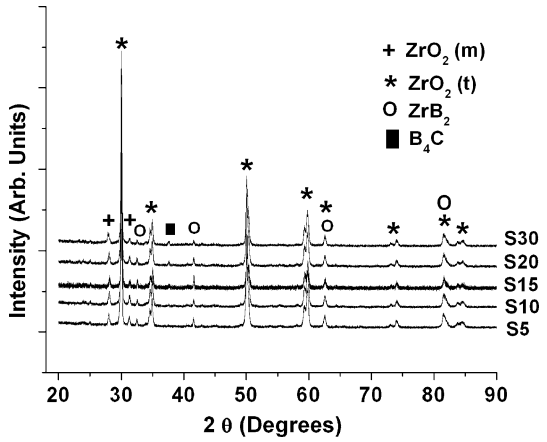

Fig. 4 XRD patterns of the sprayed coatings with respect to 5, 10, 15, 20 and 30 wt.% B_4C addition to ZrO_2 (t, tetragonal; m, monoclinic)

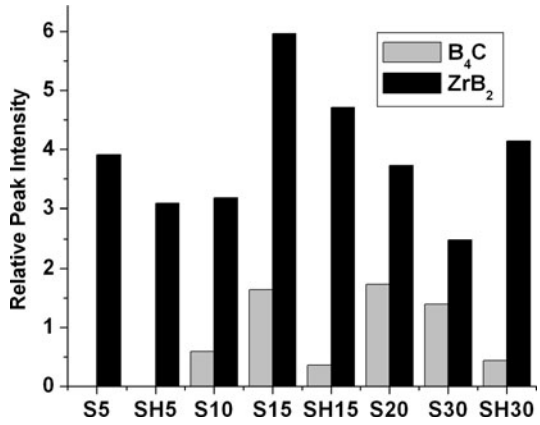

Fig. 5 The relative XRD peak intensities of ZrB_2 and B_4C of the sprayed coatings at different hydrogen flow rates (series 1 and 2)

almost all of the B_4C is consumed in the process. As the amount of B_4C in the powder mixture increases, significant breakup of the splats is observed, resulting in the formation of fine particles and a more porous microstructure (Fig. 3b, c). Coating S15 in Fig. 3(b) shows no splat morphology and the corresponding microstructure was almost comparable to loosely sintered aggregate of fine particles. From the XRD studies, the relative peak intensity of B_4C (JCPDS: 34-0798) was maximum for S20 and then decreased for S30 (2θ-37.4°), whereas the relative peak intensity for ZrB_2 was decreasing from S15 to S30 (2θ-41.7°). Maximum peak intensity for ZrB_2 was observed for S15. The relative peak intensities of B_4C and ZrB_2 obtained under similar XRD parameters for all coatings (S5-S30) are shown in Fig. 5. The maximum intensity peak of ZrO_2 at 30.04° was compared with the maximum intensity peaks of B_4C and ZrB_2 at 37.67° and 41.58° respectively for calculating relative peak intensity. Hardness measurement could not be made for the series 1 coatings because of the porous nature of the coatings and poor inter particle bonding.

3.2 Effect of Increased Secondary Gas (H_2) Flow

As described in Sect. 3.1, spray coatings with a lower H_2 flow rate of 7.08 SLM (series 1), resulted in coatings containing fine particles, a porous microstructure and a lack of structural integrity. To improve the structure of the coatings, another series of coatings were prepared using a higher flow rate for H_2, the secondary plasma gas. The H_2 flow rate was increased from 7.08 to 11.8 SLM keeping all other spray parameters constant (series 2). As discussed above, no retained B_4C was seen in S5, whereas coatings S15 and S30 showed the highest and lowest relative peak intensities for ZrB_2 respectively. Therefore, mixed powders containing 5, 15 and 30 wt.% B_4C were selected for spraying under the increased H_2 flow rate. Figure 6 shows the microstructure of the polished surface of SH5, SH15 and SH30 coatings. The cross-section of the coating SH5 is shown in Fig. 7. XRD analysis (Fig. 8, 2θ range of 34-44°) shows the presence of only ZrO_2 and ZrB_2 phases with negligible presence of B_4C. Figure 9 shows the EDS elemental mapping of zirconium, boron and oxygen for the as-sprayed SH15 coating. The boron-rich regions indicate the formation of ZrB_2. In contrast to coatings S10-S30, series 2 did not show the presence of any significant amount of unreacted B_4C. The relative peak intensities of ZrB_2 and B_4C (Fig. 5) show that coating SH15 exhibits the highest peak intensity for ZrB_2, similar to coating S15.

3.3 Hardness

As described in Sect. 3.1, the hardness of series 1 coatings could not be measured as the samples have poor inter-particle bond strength. On the other hand, when sprayed under increased hydrogen flow rate (series 2), the sprayed samples exhibited good inter-particle bonding making it possible to measure the hardness. Figure 10(a) shows a typical Vickers indentation on the surface of the coating SH5 with a 1.94 N load. The hardness values of SH5, SH15 and SH30 are presented in Fig. 10(b). The data represent the average of five indentations with standard deviation. It can be observed that the hardness of the composite coatings decreased from SH5 to SH30. The

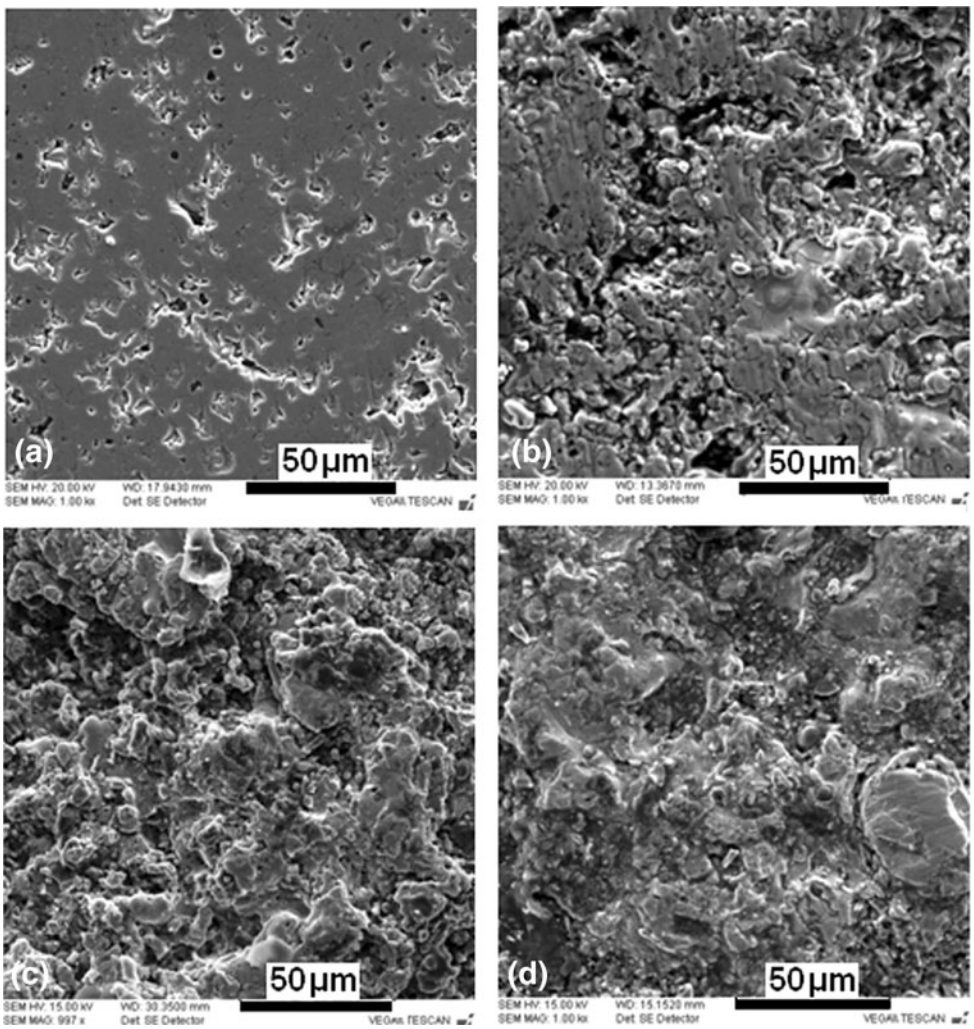

Fig. 6 Surface microstructure of polished plasma sprayed coatings of (a) ZrO_2 and (b) 5, (c) 15, and (d) 30 wt.% addition B_4C with increased hydrogen flow rate (series 2)

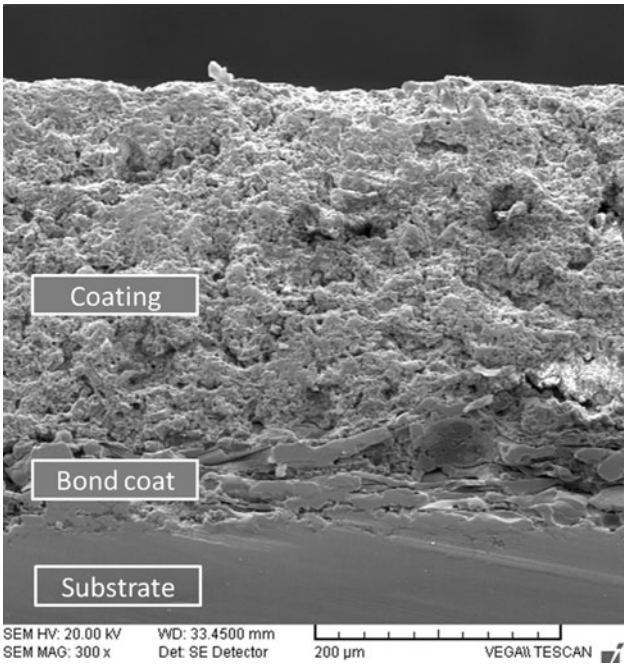

Fig. 7 Cross-section of the coating with 5 wt.% B_4C addition with increased hydrogen flow low rate (SH5)

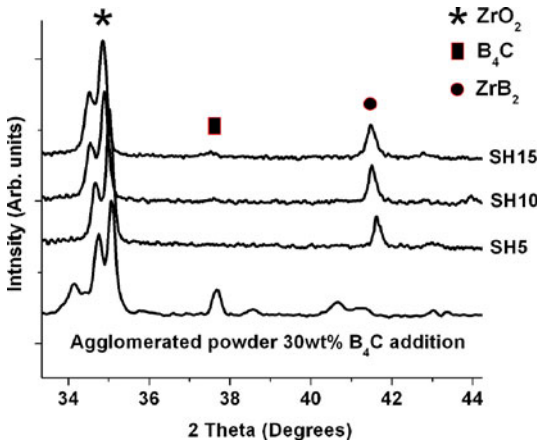

Fig. 8 XRD patterns of the plasma sprayed coatings with respect to 5, 15, and 30 wt.% B_4C addition with increased hydrogen flow rate (series 2)

hardness of the ZrO_2 coating was 659 Hv at a load of 1.94 N. All composite coatings have showed a lower hardness than ZrO_2. The lowest hardness of 163 Hv was observed for the coating SH15.

4. Discussion

Most of the research work on ZrO_2-B_4C reaction has been carried out for synthesis of borides using powder processing techniques. Some of these observations such as the nature of the reaction between the reactant particles and the effect of temperature can be applied to the plasma spraying process. The possible reactions between ZrO_2 and B_4C are as follows:

$$8ZrO_2 + 5B_4C \rightarrow 8ZrB_2 + 5CO_2 + 2B_2O_3 \quad \text{(Eq 1)}$$

$$7ZrO_2 + 5B_4C \rightarrow 7ZrB_2 + 5CO + 3B_2O_3 \quad \text{(Eq 2)}$$

$$3ZrO_2 + 2B_4C \rightarrow 3ZrB_2 + 2CO_2 + 2BO \quad \text{(Eq 3)}$$

$$5ZrO_2 + 4B_4C \rightarrow 5ZrB_2 + 4CO_2 + 6BO \quad \text{(Eq 4)}$$

Weight loss experiments carried out for hot-pressed ZrO_2 and B_4C have shown that Eq 4 is followed where the weight loss was attributed to the formation of BO and CO_2 gases (Ref 24). These solid-state reactions are endothermic, occurring at 2000 °C with reaction times of 2-5 h for the synthesis of ZrB_2. The APS process differs significantly in many respects with sintering studies. In APS process, the particle spends much less time in the hot plasma plume compared to that of a ZrO_2-B_4C sintering cycle. However, the exposed temperature of this hot zone is very high compared to sintering studies, from 6000 to 15000 °C (Ref 25). For a spraying distance of 100 mm and particle velocities of 125 m/s, the time spent by a particle in plasma is estimated to be less than 8×10^{-4} s (Ref 26). The particle temperature is estimated to be about 2760 °C (Ref 25). At this temperature, both the B_4C and ZrO_2 particles would be in a liquid state and so react rapidly in-flight in the plasma plume, resulting in the in situ formation of ZrB_2. Coating S5 (Fig. 3a) shows a significant amount of splat morphology, whereas coating S30 shows higher porosity and a uniform distribution of fine particles. There are two possible reasons for the development of porosity in these coatings. The ZrB_2 which is formed in the plasma plume does not form a splat. This is because of the high melting point of ZrB_2 and less in-flight time in the plasma. Secondly, if the reaction described by Eq 4 continues after deposition, gases would be produced within the coating. The presence of ZrB_2 is indicative of the extent of reaction between ZrO_2 and B_4C, which in turn has a bearing on the porosity and formation of fine particles. The ZrB_2 peak intensity increases, except for S10, from S5-S15 and then decreases for S20 and S30. This indicates that the size, shape of the agglomerates and the distribution of B_4C in the agglomerates (Fig. 2) is influencing the composition as well as the microstructure of the coatings. The presence of retained B_4C from coating S10 onwards indicates that de-agglomeration is taking place in the plasma and is influencing the extent of the reaction.

For series 2 coatings, the H_2 flow rate was increased. With the increase in the H_2 flow rate, the thermal conductivity and plasma to particle heat transfer increase sharply, thereby increasing the particle temperature (Ref 27). This increases the inter-particle bond strength in the coating. The presence of a low amount of retained B_4C in series 2 coatings indicates that the H_2 flow rate is influencing the reaction between B_4C and ZrO_2 in the plasma. In the coating SH5, complete reaction has

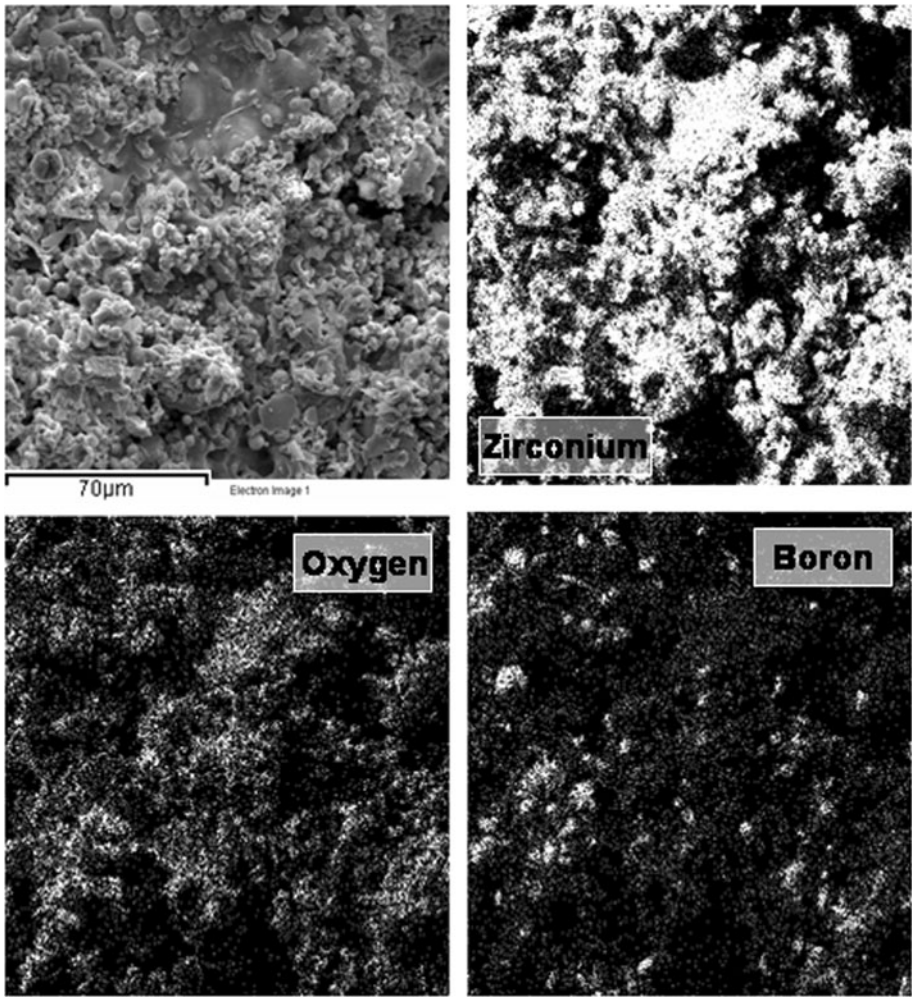

Fig. 9 EDS elemental mapping of zirconium, oxygen and boron for as sprayed composite coating with 15 wt.% B_4C addition under increased hydrogen flow rate (series 2)

occurred between B_4C and ZrO_2 while coatings SH15 and SH30 showed only a small amount of residual B_4C.

B_4C is harder than ZrO_2 and its addition to ZrO_2 is expected to increase the hardness. Also, the hardness of ZrB_2 is higher than ZrO_2. Thus, the resulting composite coating should have hardness higher than ZrO_2. However, from Fig. 10(b), it is clear that the hardness of the composite coatings is lower than the ZrO_2 coating with SH15 showing the lowest hardness (163 Hv). This is because of the higher porosity. The peak intensity of ZrB_2 is highest for SH15 (Fig. 5), which also exhibits the lowest hardness. This indicates that the amount of porosity increases with increased formation of ZrB_2, i.e. more extensive reaction between ZrO_2-B_4C.

5. Conclusions

The composite coatings deposited from mixed ZrO_2 and B_4C by APS exhibited a porous microstructure with a uniform distribution of fine particles, particularly at high amounts of B_4C. This is due to the reaction between ZrO_2 and B_4C particles occurring in the plasma resulting in the formation of ZrB_2 with an increase of the porosity. With a hydrogen flow rate of 7.08 SLM, no B_4C was observed for 5 wt.% B_4C addition. On the other hand, in all the other cases (10-30 wt.% B_4C), the coatings showed the presence of ZrB_2 and unreacted B_4C. A B_4C content of 15 wt.% in the powder yielded the maximum amount of ZrB_2 in the coating with B_4C and ZrO_2. It was observed that as the B_4C wt.% addition increases agglomerate morphology is influencing the extent of reaction and also the composition and the microstructure of the coating. Increased hydrogen flow rate resulted in superior coatings. The 15 wt.% B_4C powder mixture showed the maximum amount of ZrB_2 in the coating. No significant amount retained B_4C was observed in the coatings. The resultant coatings were a mixture of ZrB_2 and ZrO_2 phases. The Vickers hardness of the composite coatings was lower than ZrO_2 coating due to higher porosity. The lowest hardness was observed for the

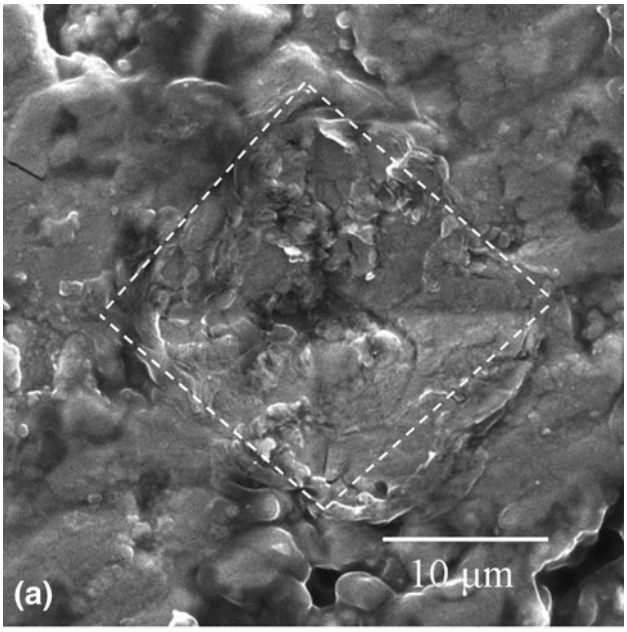

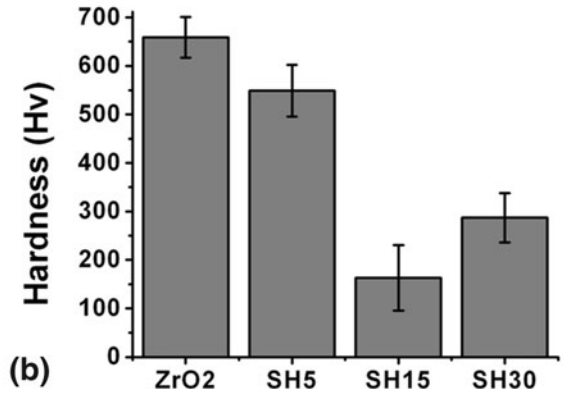

Fig. 10 (a) Vickers indentation at 1.94 N load of 5 wt.% B_4C addition, (b) Vickers hardness of ZrO_2, 5, 15, and 30 wt.% B_4C additions (series 2) of the coating surface

coating which has highest amount of ZrB_2 (15 wt.% B_4C), indicating the presence of increased porosity.

References

1. A. Vaidya, V. Srinivasan, T. Streibl, M. Friis, W. Chi, and S. Sampath, Process Maps for Plasma Spraying of Yttria-Stabilized Zirconia: An Integrated Approach to Design, Optimization and Reliability, *Mater. Sci. Eng. A*, 2008, **497**(1-2), p 239-253
2. M. Friis and C. Persson, Control of Thermal Spray Processes by Means of Process Maps and Process Windows, *J. Therm. Spray Technol.*, 2003, **12**(1), p 44-52
3. S.V. Joshi and M.P. Srivastava, Plasma Spraying of WC-Co Part II: Experimental Study of Particle Deposition and Coating Microstructure, *J. Therm. Spray Technol.*, 1993, **2**(2), p 133-136
4. E. Sanchez, E. Bannier, V. Cantavella, M.D. Salvador, E. Klyatskina, J. Morgiel, J. Grzonka, and A.R. Boccaccini, Deposition of Al_2O_3-TiO_2 Nanostructured Powders by Atmospheric Plasma Spraying, *J. Therm. Spray Technol.*, 2008, **17**(3), p 329-337
5. W. Feng, D. Yan, J. He, X. Li, and Y. Dong, Reactive Plasma Sprayed TiN Coating and Its Tribological Properties, *Wear*, 2005, **258**(5-6), p 806-811
6. P.V. Ananthapadmanabhan, P.R. Taylor, and W. Zhu, Synthesis of Titanium Nitride in a Thermal Plasma Reactor, *J. Alloys Compd.*, 1999, **287**(1-2), p 126-129
7. M. Yamada, T. Yasui, M. Fukumoto, and K. Takahashi, Nitridation of Aluminum Particles and Formation Process of Aluminum Nitride Coatings by Reactive RF Plasma Spraying, *Thin Solid Films*, 2007, **515**(9), p 4166-4171
8. Y. Motohiro, I. Tatsuya, F. Masahiro, and Y. Toshiaki, Fabrication of Silicon Nitride Thick Coatings by Reactive RF Plasma Spraying, *Mater. Trans.*, 2004, **45**(12), p 3304-3308
9. M. Yamada, Y. Kouzaki, T. Yasui, and M. Fukumoto, Fabrication of Iron Nitride Coatings by Reactive RF Plasma Spraying, *Surf. Coat. Technol.*, 2006, **201**(3-4), p 1745-1751
10. Y. Tsunekawa, M. Okumiya, T. Kobayashi, M. Okuda, and M. Fukumoto, Chromium-Nitride In Situ Composites with a Compositional Gradient Formed by Reactive DC Plasma Spraying, *J. Therm. Spray Technol.*, 1996, **5**(2), p 139-144
11. A. Fridman, Plasma Chemistry, Cambridge University Press, Cambridge, 2008
12. R.W. Smith and Z.Z. Mutasim, Reactive Plasma Spraying of Wear-Resistant Coatings, *J. Therm. Spray Technol.*, 1992, **1**(1), p 57-63
13. Y. Tsunekawa, K. Gotoh, M. Okumiya, and N. Mohri, Synthesis and High-Temperature Stability of Titanium Aluminide Matrix In Situ Composites, *J. Therm. Spray Technol.*, 1992, **1**(3), p 223-229
14. S.C. Deevi, V.K. Sikka, C.J. Swindeman, and R.D. Seals, Reactive Spraying of Nickel-Aluminide Coatings, *J. Therm. Spray Technol.*, 1997, **6**(3), p 335-344
15. S. Dallaire and G. Cliche, Tribological Properties of TiC-Fe Coatings Obtained by Plasma Spraying Reactive Powders, *J. Therm. Spray. Technol.*, 1993, **2**(1), p 39-44
16. P.V. Ananthapadmanabhan and P.R. Taylor, Titanium Carbide–Iron Composite Coatings by Reactive Plasma Spraying of Ilmenite, *J. Alloys Compd.*, 1999, **287**(1-2), p 121-125
17. Y. Dong, D. Yan, J. He, X. Li, W. Feng, and H. Liu, Studies on Composite Coatings Prepared by Plasma Spraying Fe_2O_3–Al Self-Reaction Composite Powders, *Surf. Coat. Technol.*, 2004, **179**(2-3), p 223-228
18. A. Ohmori, S. Hirano, and K. Kamacta, Spraying TiN by a Combined Laser and Low-Pressure Plasma Spray System, *J. Therm. Spray Technol.*, 1993, **2**(2), p 137-144
19. C. Tekmen, Y. Tsunekawa, and M. Okumiya, In-Situ TiB_2 and Al_2O_3 Formation by DC Plasma Spraying, *Surf. Coat. Technol.*, 2008, **202**(17), p 4170-4175
20. J.J. Moore and H.J. Feng, Combustion Synthesis of Advanced Materials: Part-1. Reaction Parameters, *Prog. Mater. Sci*., 1995, **39**(4-5), p 275-316
21. A. Goldstein, Y. Yeshurun, and A. Goldenberg, B_4C/Metal Boride Composites Derived from B_4C/Metal Oxide Mixtures, *J. Eur. Ceram. Soc.*, 2007, **27**(2-3), p 695-700
22. F. Mizusako, H. Tamura, K. Horioka, and Y. Harada, Zr–O–B Ceramics/Ni–20%Cr Alloy Graded Coating Produced by Electrothermal Explosion Spraying, *Surf. Coat. Technol.*, 2004, **187**(2-3), p 257-264
23. A.L. Chamberlain, W.G. Fahrenholtz, and G.H. Hilmas, Pressureless Sintering of Zirconium Diboride, *J. Am. Ceram. Soc.*, 2006, **89**(2), p 450-456
24. H. Kim, Y. Koh, and H. Kim, Reaction Sintering and Mechanical Properties of B_4C with Addition of ZrO_2, *J. Mater. Res.*, 2000, **15**(11), p 2431-2436
25. J.R. Davis, *Hand Book of Thermal Spray Technology*, J.R. Davis, Ed., ASM International, Materials Park, 2005, p 5
26. A. Kulkarni, Z. Wang, T. Nakamura, S. Sampath, A. Goland, H. Herman, J. Allen, J. Ilavsky, G. Long, J. Frahm, and R.W. Steinbrech, Comprehensive Microstructural Characterization and Predictive Property Modeling of Plasma-Sprayed Zirconia Coatings, *Acta Mater.*, 2003, **51**(9), p 2457-2475
27. A. Kulkarni, A. Vaidya, A. Goland, S. Sampath, and H. Herman, Processing Effects on Porosity-Property Correlations in Plasma Sprayed Yttria-Stabilized Zirconia Coatings, *Mater. Sci. Eng. A*, 2003, **359**(1-2), p 100-111